Bulletin of Department of Geology, Tribhuvan University, Kathmandu, Nepal, vol. 23, 2022, pp. 1-10
DOI: https://doi.org/10.3126/bdg.v23i1.64679

Rockmagnetic Characterization of the Quaternary Fluviolacustrine Sediments of the Thimi Section, Kathmandu Valley, Nepal

Pitambar Gautam[1]*, Ghanashyam Neupane[2], Pascale Huyghe[3], Pierre Rochette[4] and Yaeko Igarashi[5]

1. The Hokkaido University Museum, Hokkaido University, N10 W8, Sapporo 060-0810, Japan.
2. Idaho National Laboratory, Idaho Falls, ID 83404, USA.
3. Institut des Sciences de la Terre, Université Grenoble Alpes, Grenoble Cedex 9, France.
4. Aix-Marseille Universite, CNRS, IRD, INRAE, UM 34 CEREGE, Aix-en-Provence, France.
5. Institute of Low-temperature Science, Hokkaido University, Sapporo 060-0810, Japan.

ABSTRACT

The fine-grained silt/clay sediments sampled at 38 levels of a 21 m thick segment at the Thimi outcrop in the Kathmandu valley have been studied for their rockmagnetic properties. These sediments have yielded consistently normal magnetic polarity and ^{14}C ages determined by various workers between 20 and 45 kyrs or even more. They were measured for a set of rock magnetic parameters: low-field magnetic susceptibility, parameters derived from isothermal remanent magnetization (IRM) acquisition and demagnetisation ($IRM_{0.3T}$, IRM_{3T}, MDF_{IRM}), anhysteretic remanent magnetization (ARM) (ARM_{tot}, ARM(30 mT)/ARM_{tot}, χ_{ARM}), hysteresis parameters, etc. Several relationships between these parameters have been suggested for the Kathmandu valley sediments. Four rockmagnetic zones, based on the minor variations in magnetic mineral types and grain size parameters, are proposed and their possible relationship to the published pollen data has been discussed.

Keywords: Rockmagnetic parameters; Environmental magnetism; Magnetic susceptibility; Kathmandu valley; Quaternary; Lake sediments

Received : 13 July 2022 Accepted: 4 December 2022

INTRODUCTION

The lacustrine, fluvial, and deltaic sediments (>300 m thick) deposited in the Pliocene-Pleistocene paleo-Kathmandu intermontane basin (present-day area: 650 km^2; average elevation of the valley floor: 1,340 m; elevation of highest mountains surrounding the basin: >2,700 m) are regarded by geoscientists as the natural archive of the history of Himalayan uplift and the paleoclimate. The lake sediments indeed provide information on climate conditions at local, regional, and global scales but the extent of information that can be extracted is dependent on the location, configuration of the depobasin and the catchment, duration of deposition, completeness of the depositional record, changes in the sediment provenance, and the response of the proxy parameters to the paleoenvironmental conditions that include climatic, tectonic, as well as hydrological regimes (see Verosub and Roberts, 1995, for a review). As these parameters vary in each individual case, detailed studies of the available sedimentary record together with deciphering of chronology and examination of the various possible proxy parameters are indispensable.

The Kathmandu basin continues to be the target of sediment geological studies by the global research community aiming at reconstructions in terms of geography, environment, climate, hydrology, and tectonic processes of the past as well as attempts to make inferences for the present and future phenomena (Sakai, 2001; Sakai et al., 2001; Dill, 2006; Mugnier et al., 2011; Sakai et al., 2016; Paudel, 2022). In this study, we focus on magnetism of sediments with the aim of deriving rockmagnetic parameters as paleoenvironment/paleoclimate proxies and establishing a magnetic polarity sequence for determining the depositional chronology of the sedimentary succession. The rock magnetic parameters reflect the magnetic signal contributed by detrital inputs (mineralogical composition and grain size), organic productivity, microbial activity, weathering or early diagenesis

*Corresponding author:
E-mail: pitambargautam@yahoo.co.jp (Pitambar Gautam)

and so on. A relatively short section near Thimi that has some chronological constraints, continuous exposure and abundance of the fine-grained lacustrine layers, and the horizontal bedding that is laterally persistent over hundreds of meters (Dill et al., 2001; Gautam et al., 2001). The Thimi section considered belongs to the Thimi and/or Gokarna Formation(s) of the 'younger stage deposits', which are represented by fluvio-lacustrine and delta-plain facies (Yoshida and Igarashi, 1984; Sakai, 2001) (Fig. 1). Supported by a normal magnetic polarity record and several radiocarbon (^{14}C) dates, these facies were assigned <30,000 yrs (Yoshida and Igarashi, 1984).

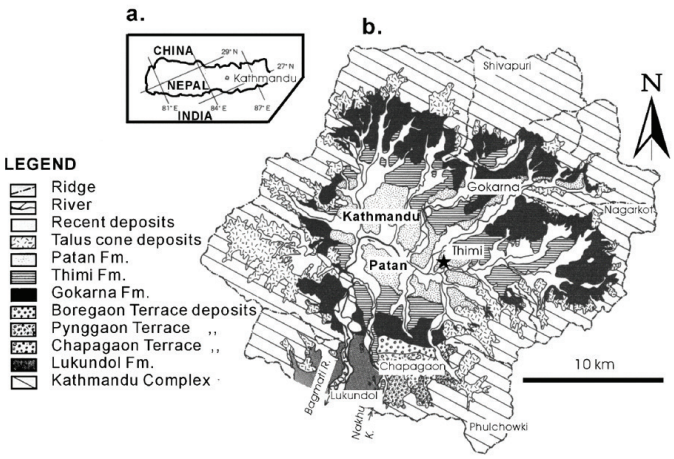

Fig. 1. (a) Sketch map of Nepal showing the position of Kathmandu. (b) generalized geological map of the Kathmandu valley (adapted from Yoshida and Gautam, 1988) showing the location of section studied at Thimi marked by a star.

The study on magnetic polarity of sediments is aimed at refining the existing remanent magnetization record for a better chronological resolution (e.g., detection of the subtle variations in the remanence record including possible reversals that could verify the validity of reported radiometric dates) and obtaining fundamental rockmagnetic parameters and describing them in terms of the nature (type, quantity, grain size, domain state) of the magnetic minerals.

LITHOLOGY AND AGE OF THE THIMI SECTION

A simplified litholog of the Thimi section exposed at a quarry (lat: 27°40.538'N, long: 85°23.467'E) is shown in Fig. 2. The upper part is attributable to the Thimi Formation (*sensu* Yoshida and Igarashi, 1984) as the top of the section is at ca. 1,326 m and closer to the Thimi geomorphic surface with altitude range of 1,330–1,340 m. The lower part may belong to the Gokarna Formation. The sediments comprise channel sands, lacustrine and flood plain deposits, characterized by low sand/(silt+clay) ratio but a variable spectrum of sedimentary features, described as 'Unit II: fine-grained facies' by Dill et al. (2001). The thickness of the fine sand, silt and clay layers ranges from a few cm to several dm. The top layer, immediately underlying the topsoil, is represented by diatomite. In adjoining areas to the West, Sakai et al. (2001) described similar sections as delta plain facies comprising several sedimentary cycles of sand beds (coarse-sediment interval) and alternation of fine to very fine sand and silt beds (fine-sediment interval). Each sedimentary cycle corresponds to an event of a small-amplitude lake level rise and fall sequence superposed on a long-term lake level rise trend of the paleo-Kathmandu lake.

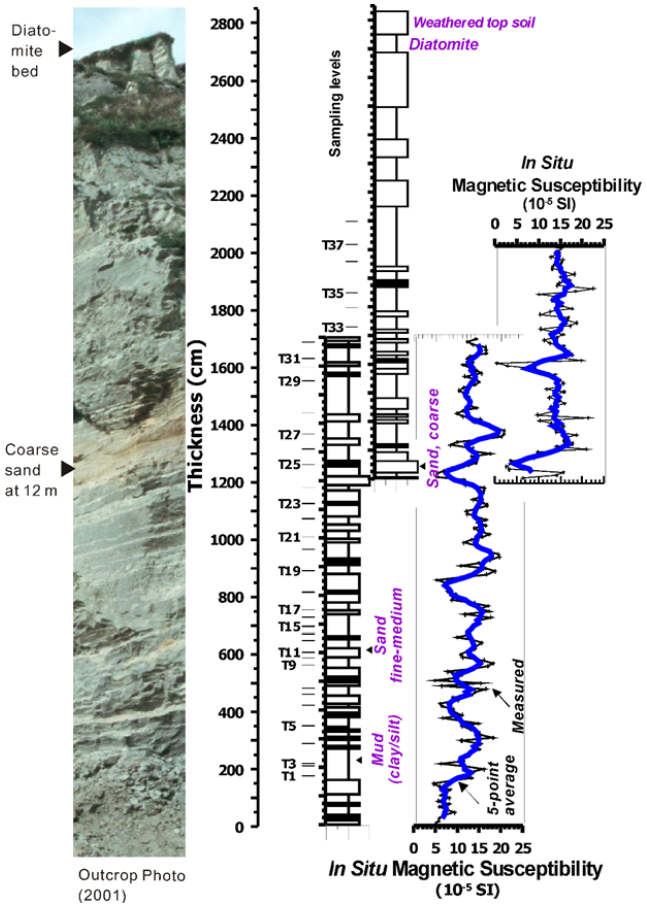

Fig. 2. Simplified lithologs of the section (middle) belonging to 'the younger stage deposits' exposed at Thimi quarry with two sub-sections, which are separated by ca. 20 m and the one in the right side is towards the NE. Variation of the low-field magnetic susceptibility measured in situ in two sub-sections is shown in the right side. The upper half of the partial photograph of the outcrop (shown in the left, with approximately same scale with the logs) corresponds to the litholog in the right side (base at about 12 m). The medium-to-coarse grained sand layer at 12 m height is laterally traceable and also distinctly marked by very low susceptibility. T1-T38: levels of samples taken for laboratory measurements.

Using a normal magnetic polarity record attributable

to the Brunhes Chron (< 0.733 Ma) and several radiocarbon (^{14}C) dates, the following age ranges were assigned to the Formations constituting the younger stage deposits: 30,000-28,000 yrs. BP for Gokarna Formation; 28,000–24,000 yrs. BP for Thimi Formation; and 19,000–11,000 yrs. BP for Patan Formation (Yoshida and Igarashi, 1984; Yoshida and Gautam, 1988). There are additional reported ^{14}C ages older than 30,000 yrs. BP for Thimi section: (i) 45,300±6100/3400 yrs. BP mentioned in Igarashi et al. (1988) but suspected to represent the age of the wood fragment derived from older deposits; (ii) 45,140±1,310 yrs. BP and 43,180±1,310 yrs. BP for two carbonaceous samples corresponding to ca. 4 m and 15 m levels, respectively, in the present section (see Fig. 2) (Gajurel, 1998); and (iii) 41,700±5600/3200 and >37,900 yrs. BP, respectively, for two wood samples collected at 13 m and 21 m depths from the top of the exposure (Paudayal and Ferguson 2004). These data constrain the age of the upper part of the Thimi exposure at about 41,000 to 43,000 yrs. BP. The age of lower part of the exposure, however, seems to be beyond the limit of the radiocarbon method.

However, samples of the plant debris collected from the fine-grained sediments at the lower part of the Thimi quarry have yielded varying ages: 25,815±1,665 yrs. BP (Dill et al., 2001) and 29,290±1,390 yrs. BP and 38,265±1,230 yrs. BP (P. Huyghe, unpublished data) (Fig. 2). The variable ages may stem, in part, from the fact that erosional surfaces differing in age, by their location, are highly developed in the late Pleistocene younger stage deposits underlying the morphological Thimi and Gokarna surfaces. Some ^{14}C dates for wood fragments, derived from older deposits, may indeed be older than the real ages of deposition of the host sediments. On the other hand, the standard errors assigned to some of these dates, in general, also seem to be rather high to justify their validity. In the absence of objective criteria to judge for or against these dates, the age of the Thimi section may be regarded to lie within 50,000–20,000 yrs. BP.

SAMPLING AND LABORATORY PROCEDURE

First of all, the variation of *in situ* low-field volume magnetic susceptibility (κ_{lf}) along the section was measured using a portable susceptibility-meter (WSL-A, Aerogeophysical Survey of China) with 10-cm spacing.

For measurements at the laboratory, 38 samples were taken preferentially from the levels occupied by the dark gray silt/clay layers (lacustrine beds) with an average vertical spacing of ca. 50 cm. Cylindrical (10 cc by volume) non-magnetic polyethylene boxes were pressed, with their open-ends, into the near-vertical sediment face. Each filled box was oriented, using a magnetic compass, prior to its removal from the outcrop and then sealed with a cap so as to retain moisture and the sediment integrity.

Magnetic measurements were made at the paleomagnetic laboratory of CEREGE, France. The experiments conducted (equipment) and procedures are as follows:

(i) ***Natural remanent magnetization (NRM)*** measurements employing stepwise alternating field demagnetization (AFD) (2G Enterprises 755R DC SQUID magnetometer, with noise level <0.01 mAm^{-1}, equipped with static tri-axial demagnetisers). Each specimen was demagnetized at peak fields ranging between 0 and 100 mT at 14 steps (5 mT increment below 50 mT and 10 mT thereafter). The NRM directions were analysed using the PALMAG program of Munich University, which has the option for line-fitting through principal component analysis (Kirschvink, 1980).

(ii) Measurements of the ***low-field magnetic susceptibility (χ_{lf})*** of all specimens (AGICO KLY-2 Kappabridge) and the thermal variation of the susceptibility using limited subsamples (about 0.5 cm^3) with the aid of the CS-2 furnace.

(iii) ***Isothermal remanent magnetization (IRM)*** acquisition at selected fields of 0.3 T, 1.5 T and 3 T on all standard specimens (Magnetic Measurements pulse magnetizer) to differentiate the magnetic minerals (Dunlop and Özdemir, 1997) and subsequent measurement of the acquired remanence using the SQUID device. The SIRM (i.e., IRM acquired at 3T denoted also as IRM_{3T}) was subsequently demagnetised by single-axis AFD (with 5 mT steps between 50 and 100 mT, but rarer steps outside this range) in order to determine the medium destructive field (MDF_{IRM} = magnitude of the peak AF required to reduce the IRM moment to half of its initial value).

(iv) ***Anhysteretic remanent magnetization (ARM)*** acquisition at 100 mT peak AFD and a bias field of 0.47 Oe (the SQUID device equipped with coil to create DC fields). The acquired ARM_{tot} was subsequently demagnetised at 30, 50 and 70 mT peak fields.

(v) Measurements of ***magnetic hysteresis and backfield destruction of the remanence*** on subsamples (0.15–0.25 g) from eight levels (Micromag-2900). The hyteresis data were processed by the "hystear" program of Dobenec (1996).

RESULTS AND INTERPRETATION

In situ low-field magnetic susceptibility

The *in situ* κ_{lf} varies between 0.4 x 10^{-5} and 22.6 x 10^{-5} SI with very close inverse relationship to the macroscopic grain size: low for sands, intermediate for silts and high for black clay/silty clays (Fig. 2). In general, κ_{lf} for finer sediments has less fluctuation with height than for sands, for which the susceptibility tends to decrease upwards. This seems to correlate with the increase in the grain size of sands and also the relative proportion of quartz with height. The cyclic nature of the susceptibility is dictated by the rhythmic variation of the sediments. The silt/clay layers sampled for study of polarity and rockmagnetic parameters had in general κ_{lf} exceeding 10 x 10^{-5} SI.

Magnetic remanence data

The NRM intensity of 38 specimens ranged between 0.09 to 0.65 mA m^{-1} with an average value of 0.29±0.13 mA m^{-1}. The semi-consolidated nature of the sediment samples (the water content was up to 17% by weight) and sampling in polyethylene cylinders permitted only AFD. As shown in Fig. 3 (a,b), the remanence decays rather fast up to 30–40 mT, followed by a slow decrease up to 60–65 mT, and then changes variably (slow increase or decrease or erratic fluctuations) in higher fields. The unstable behaviour at higher fields is believed partly due to either the drop of the remanence to the noise level of the instrument or the acquisition of the gyromagnetic remanence (Goddu et al. 2007). The first of these demagnetization ranges corresponding to low coercivity spectra implies to a soft component likely of viscous origin and carried by maghemite, soft hematite, or even magnetite. The second, or intermediate, demagnetization range corresponding to the more stable behaviour is believed to be indicative of magnetite, which is known to be the main carrier of the characteristic primary remanence in the sediments from the Southern part of the Kathmandu valley (Goddu et al. 2007). The remanence intensity left after treating specimens at 60–100 mT is up to 40% of the initial NRM and it probably rests on hematite of high

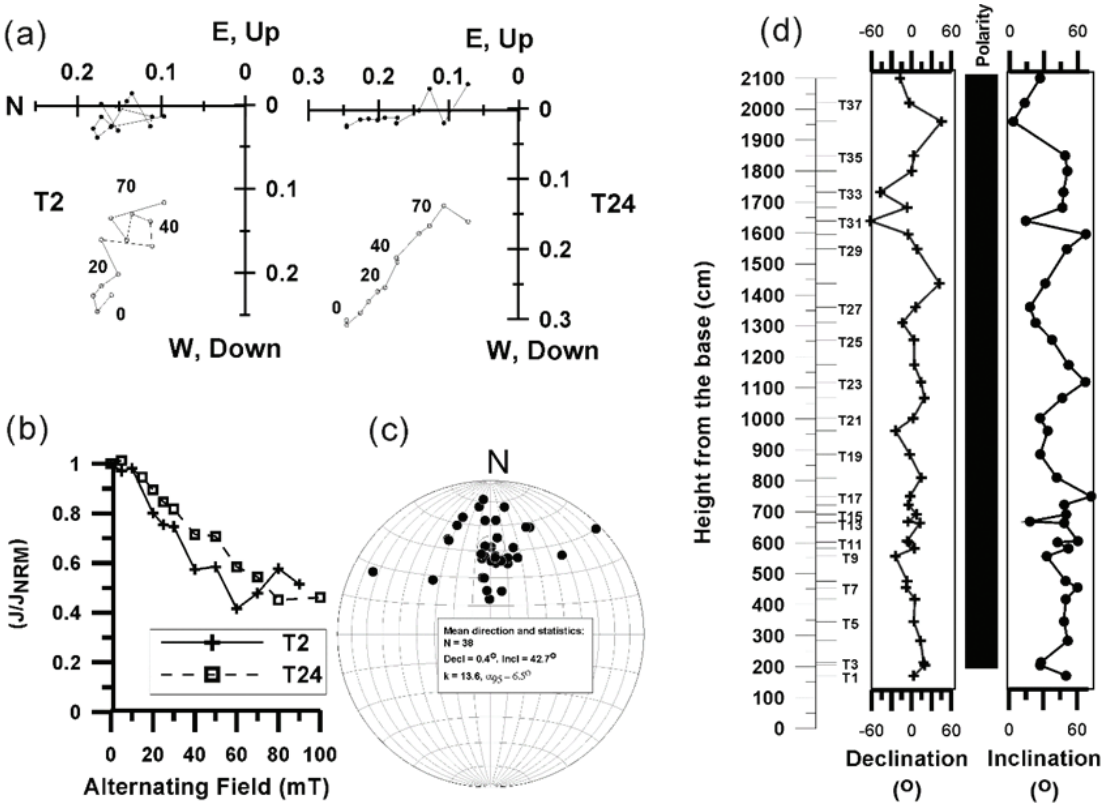

Fig. 3. Diagrams to show the nature of the *in situ* magnetic polarity record of the Thimi section. Behaviour of representative specimens (T2 and T24) during alternating field demagnetisation (AFD) is shown as orthogonal vector plots (a), and normalized intensity response curves (b). The stable characteristic remanence (ChRM) directions for all 38 samples in equal-area net are shown in (c) together with the mean direction. In (d), the magnetic polarity (consistently normal, as shown by black bar) derived from the declination and inclination of the characteristic remanence is presented.

coercivity (Fig. 3b). Thus, accurate estimation of the intermediate component is not easy because of the short range of demagnetization and the unstable demagnetization behaviour of specimens at fields higher than that range.

The IRM ratios discussed later can be used to support the inferences on magnetic minerals contributing to the remanence. The average values for $IRM_{0.3T}/IRM_{1.5T}$ and $IRM_{1.5T}/IRM_{3T}$ are 0.82 and 0.99 respectively. These values testify that soft coercivity magnetite-like phases contribute to 82% and intermediate or harder coercivity hematite-like phases – another 17%. The remaining contribution of ca. 1% may indicate contribution of very hard coercivity minerals such as goethite but is insignificant in view of the measurement accuracies and possible viscous behaviour of high-field IRM of these sediments which possess multidomain grains as shown later.

The soft component is most likely of a recent field origin. The intermediate range component is characterized as hard component. Our experience with the clastic sediments of the Siwalik Group has shown that goethite rather than hematite commonly carries a strong recent field overprint of normal polarity. As the goethite-based remanence can't be cleaned within commonly applied AFD ranges, the original ChRM may be completely masked by the overprint (Gautam and Fujiwara, 2000). However, we have no evidence of the presence of goethite in these sediments. Hence the likely candidate for the high coercivity remanence persisting above the intermediate demagnetization range is hematite.

The bedding planes shown by the prominent silt/clay layers sampled in the Thimi section are consistently horizontal (variable dip directions but angles of <3º). Therefore, *in situ* directions plotted in Fig. 3c are used for assigning polarity. Due to consistently northerly declinations and shallow to moderate inclinations (present day field at Kathmandu: D = 0º, I = 47º), all of them indicate normal polarity (Fig. 3d).

Thermal variation of the low-field magnetic susceptibility

The magnetic susceptibility vs. temperature curves (Fig. 4) show very low positive or even negative magnitudes of the initial susceptibility indicative of significant contribution of diamagnetic along with paramagnetic and ferromagnetic minerals (Hrouda, 1994). During heating, a distinct susceptibility rise occurs above 375°C. This points to formation of magnetite by decomposition of clay minerals or pyrite. Such mineralogical inferences are consistent with the average mineralogical composition of the Kathmandu valley sediments (similar to those in Thimi section): 80% - quartz, feldspar, and mica; 20% - mainly clay minerals (illite, smectite, illite-smectite and chlorite-smectite mixed layers, kaolinite and chlorite, in decreasing importance) (Fujii et al., 2001; Kuwahara et al., 2001; Gajurel, 1998). Another possible candidate responsible for the susceptibility rise is greigite, which occurs in the younger stage sediments of the Kathmandu Valley (Gautam et al., 2001). The significant susceptibility change (drop/rise upon heating/cooling) at about 580°C is evidence for the occurrence of original and/or newly produced magnetite.

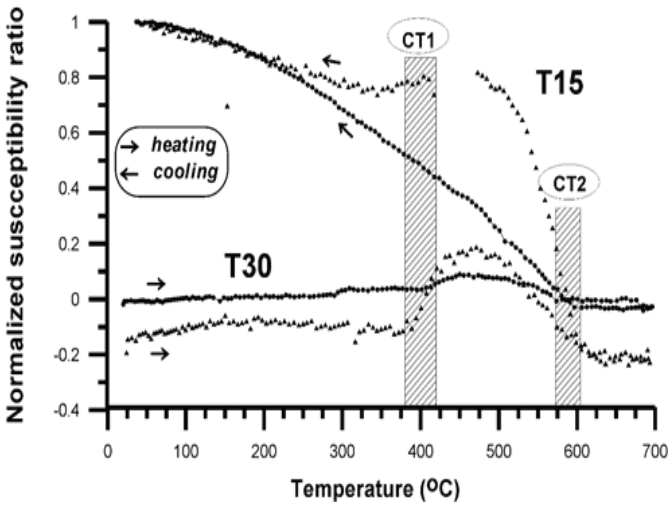

Fig. 4 : Magnetic susceptibility vs. temperature curves (experiments conducted in air). CT1 and CT2 are the intervals of distinct rise and drop of susceptibility. These intervals seem to be related to mainly magnetite, pre-existing and newly formed by transformation of clay minerals, as shown by the heating and cooling curves. Note that the susceptibility in each curve is normalized to the maximum value.

Hysteresis characteristics

As all eight samples had identical hysteresis characteristics, the measured total hysteresis loop and backfield curve (within applied field of ±1 T) together with the calculated saturation asymptote and separated ferromagnetic hysteresis curve for one sample (Fig. 5a). Table 1 shows hysteresis parameters estimated using the synthetic ferromagnetic hysteresis and backfield curves like those given in Fig. 5b&c, following Dobenec (1996). The average values of coercive force (B_c) and coercivity of remanence (B_{cr}) are low with 8.83±1.10 and 39.92±4.61 mT, respectively. In conjunction with the extremely low ratio of the saturation remanent magnetization (M_r) and the

saturation magnetization (M_s), they point to the predominant ferromagnetic mineral being magnetite with grain size in multidomain zone (Day et al. 1977) (Fig. 5d).

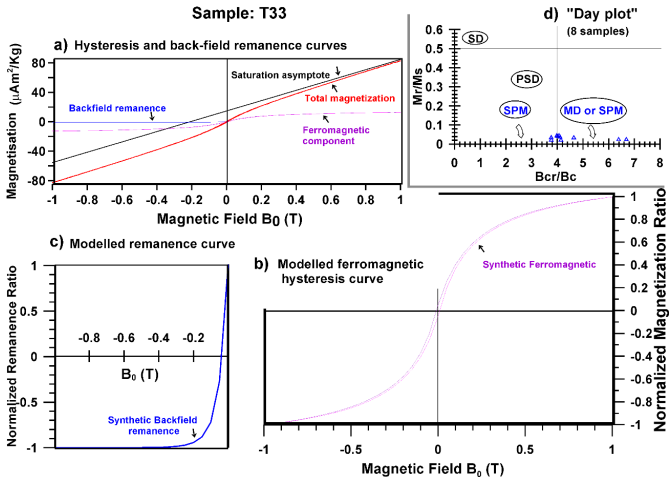

Fig. 5: Experimental and separated hysteresis and back-field magnetization curves (a), together with simulated ferrimagnetic hysteresis (b), and back-field remanence curves (c). The "Day plot" based on hysteresis parameters of 8 samples presented in (d) indicates the contribution from the superparamagnetic as well as multidomain grains.

Table 1: Hysteresis Loop and Back-field remanence acquisition data

Sample	Bc	Mr/Ms	Mr/Mferro	Bcr	Bcr/Bc	Sus_{fer}/sus_{tot}
	(mT)	(%)	(%)	(mT)	(ratio)	(ratio)
T1	9.21	4.37	5.2	37.44	4.07	0.53
T5	6.97	2.33	2.9	44.54	6.39	0.32
T10	7.27	2.36	3.1	48.59	6.69	0.22
T15	8.84	3.64	4.3	36.32	4.11	0.46
T22	8.71	3.39	4.1	32.78	3.76	0.48
T30	10.32	4.01	4.7	41.41	4.01	0.52
T33	9.87	4.28	4.9	39.24	3.98	0.45
T38	9.44	2.1	2.8	39.07	4.14	0.22
Average	8.83	3.31	4	39.92	4.64	0.4
±stdev	1.1	0.87	0.89	4.61	1.1	0.12

Rockmagnetic parameters

A comparison of the IRM acquired at 0.3 T, 1.5 T and 3 T reveals that the low-coercivity (magnetite-like) soft phase contributes to 82% (78 to 91%), another relatively hard-coercivity (hematite-like) phase contributes to additional 17 % (13–21 %) with just 1 % (0–2.4 %) share of the phase with hardest coercivity (probably goethite). Assuming most of the IRM_{3T} to be contribution of two phases (soft:hard = 5:1), the ratio $IRM_{0.3T}/IRM_{3T}$ adequately describes the variation along the section. The MDF_{IRM} values show a range of 59–100 mT that contrasts with the wider range (5–100 mT) of MDF_{NRM} and there is no correlation between the two (Fig. 6a). The MDF_{IRM} shows an excellent correlation to the ratio of IRM remaining at selected moderate AF to the SIRM as illustrated by using the ratio of IRM(50) to SIRM (Fig. 6b). For such sediments, there is a clear advantage of using the ratio (e.g., IRM(50)/SIRM) over the MDF_{IRM} just to save the measurement time. Behaviour of two specimens having extreme demagnetisation response is illustrated in Fig. 6c. The NRM and IRM magnitudes remaining after demagnetisation at 100 mT are found to be up to 40%, which implies that the remanence contribution of the relatively hard magnetic phase (hematite-like) is also significant.

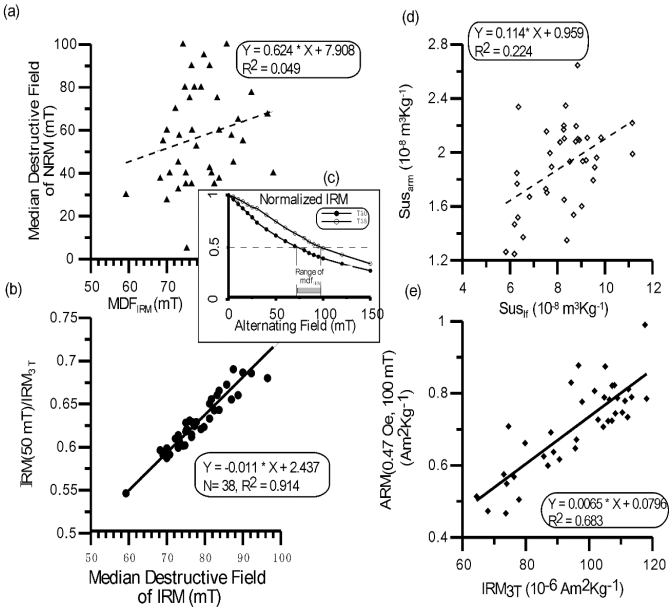

Fig. 6: Relationships between various rockmagnetic parameters. (a, b) Relationship between MDF_{NRM} (the medium destructive field of NRM) and IRM(50)/SIRM to MDF_{IRM}). (c) IRM demagnetisation curves for two specimens showing extreme MDF_{IRM} values. (d) Lack of correlation between the magnitudes of the susceptibility of anhysteretic remanent magnetization (χ_{ARM}) and the low-field magnetic susceptibility (χ_{lf}). (e) Good correlation between the ARM_{tot} and SIRM magnitudes.

Rockmagnetic zonation using multivariate statistical analysis

In order to see the variability of the magnetic signal along the Thimi section, altogether nine quantities (rockmagnetic parameters and ratios) are plotted against the thickness (Fig. 7: fundamental magnetic quantities such as NRM moment and SIRM at the left; concentration and coercivity-dependent quantities in the middle, and both concentration and grain size-dependent quantities or ratios in the right). A visual analysis reveals that the NRM moment and SIRM vary in concert with thickness and exhibit cyclic nature. Also evident are coherent variations between the magnitudes of χ_{lf} and χ_{ARM}

but the cyclic nature is less clear. However, the cyclic nature is far less evident for quantities like MDF_{IRM} and ARM(30 mT)/ARM_{tot} (an inverse measure of the magnetic hardness of the sample) though the fluctuations seem to vary by zones.

For objective rock magnetic zonation, we use multivariate statistics including principal component analysis (PCA) and cluster analysis by fuzzy c-mean method (FCM). The input data comprised a 9 x 38 matrix formed by standardized elements (the values in each column being equal to the difference from mean divided by the standard deviation of data for the corresponding parameter). Numerical calculations were made by using Matlab® commercial software.

For quantities showing regular cyclicity in these data, derived from laboratory measurements on 38 specimens, a wavelength of about 4 m is obvious. A fast Fourier transform of the in situ susceptibility data, measured at 10 cm spacing along the vertical as discussed in section 4.1, yields a most significant cycle of 397 cm and confirms this observation.

Palynological data from the Thimi section

From palynological data on 13 samples taken from the Thimi section, whose thickness was estimated to be 31 m at the then existing quarry, Igarashi et al. (1988) suggested four pollen zones: TM-1 (*Pinus-Quercus*-Pteridophyte Assemblage); TM-2 (*Quercus*-Gramineae-Pteridophyte Assemblage); TM-3 (*Pinus-Quercus*-Gramineae-Pteridophyte); and TM-4 (*Quercus-Pinus-Picea* Assemblage) (Fig. 7). For the climatic interpretation based on pollen data, the following four situations were considered:

(i) *Pinus* occurring predominantly in TM-1 and TM-3 zones has a wide vertical distribution range. The present day climate of Kathmandu valley is warm temperate at present. The valley floor (average elevation 1,340 m) is characterized by *Schima-Castanopsis* forest. *Pinus* is distributed in the surrounding mountain slopes up to 2,762 m. In Nepal, *Pinus* has much wider altitudinal range (as low as 500 m for *Pinus roxburghii* under warmer climate and as high as 4,300 m for *Pinus wallichiana* under colder climate (Polunin and Stainton, 1984). This implies that more accurate and detailed paleoclimatic reconstruction requires discrimination of different species of pine using scanning electron microscope (SEM) (Nakagawa et al., 1996; Fujii and Sakai, 2001; Paudayal and Ferguson, 2004; Paudayal, 2005). Using SEM, Paudayal and Ferguson (2004) identified more than 50% of *Pinus* pollen from the Thimi Formation as *Pinus wallichiana,*

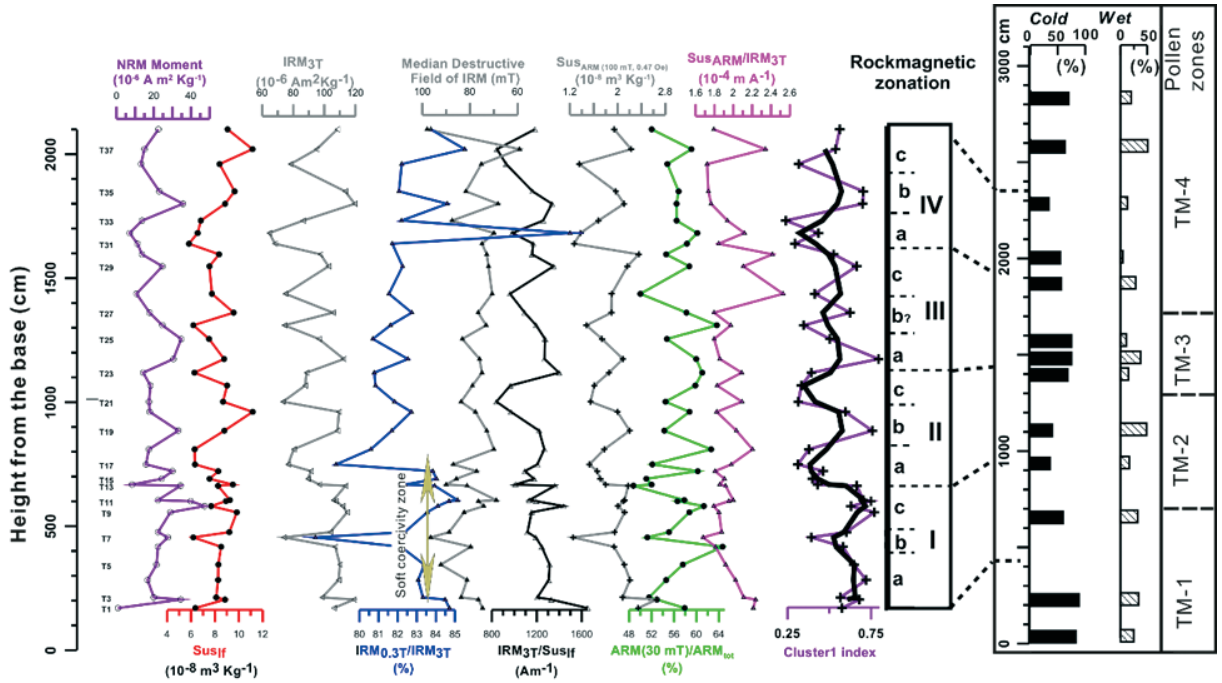

Fig. 7: Variation of selected rockmagnetic parameters of the fine-grained sediments for the Thimi section. $IRM_{0.3T}/IRM_{3T}$ marks a distinct magnetic boundary at about 7m, below which the share of soft-coercivity mineral(s) is relatively high (4th curve). In general, periodic variations (sinusoidal, with wavelength of about 4 m) in several parameters (NRM moment, IRM_{3T}, MDF_{IRM}, χ_{lf}, χ_{ARM}) are evident throughout the section. Cluster analysis of all parameters allows a more objective classification into 4 prominent rockmagnetic zones (RM-I to RM-IV), each of which consists of three (a-c) subzones. Pollen data zonation (TM-1: Pinus-Quercus-Pteridophyte Assemblage; TM-2: Quercus-Gramineae-Pteridophyte Assemblage; TM-3: Pinus-Quercus-Gramineae-Pteridophyte; TM-4: Quercus-Pinus-Picea Assemblage) for a former outcrop of the Thimi area, after Igarashi et al. (1988), with inferred correlation to the present section is also presented for comparison.

while the remaining was unidentified. Based on the altitudinal distribution range of *Pinus wallichiana,* they reconstructed the vegetation zones in the past as depressed by as little as 700 m or as much as 1750 m.

(ii) *Quercus* found to be predominant in TM-2 and TM-4 zones occurs within the present day mountain slopes in between 1,800 and 2,700 m (Sakai, 2001). However, much wider ranges of occurrences, from 450 m for *Quercus glauca* to 3,800 m for *Quercus semecarpifolia,* are known in Nepal (Polunin and Stainton, 1984). SEM-based observation of pollen from the Thimi Formation by Paudayal and Ferguson (2004) revealed that *Quercus semecarpifolia* was rare, whereas *Quercus lanata* (1,400-2,400 m) and *Quercus lamellosa* (1,600-2,800 m) were dominant. These observations suggest that the predominance of *Quercus* implies a relatively warm climate.

(iii) There are several taxa which may be used as the reliable indicators of the climatic condition. *Picea, Abies, Tsuga, Betula* and Ericaceae characterized by distribution from the upper temperate to subalpine zones serve as key genera for cold climate. Similarly, cool temperate broad-leaved trees such as *Juglans, Corylus, Ulmus, Carpinus* and *Ilex* growing in more or less restricted habitats also serve as subordinate key genera for a cooler climate.

(iv) *Alnus* and aquatics such as *Trapa, Typha, Myriophyllum, Sparganium, Nuphar, Menyanthes* and green algae *Pediastrum* indicate the existence of marshes and/or open water. The high frequency of fern spores is a key indicator of humid climate, though fern growth might have been affected by local conditions.

In this paper, we calculate two indices: 'cold', as the total counts of conifers including *Pinus* and broad-leaved trees mentioned in (iii); and 'wet', as the total of *Alnus*, Pteridophyte and aquatics mentioned in (iv). Normalization of 'cold' by the total tree pollen and 'wet' by the sum of total pollen and spores yields the indices as percentages shown in Fig. 7 (right side).

Based on the proportion of 'cold' and 'wet' percentages, climate during depositional period of the Thimi Formation may be reconstructed as follows. Climate remained relatively cooler during RM-I (and sometimes prior to it) below 7-m level, during RM-III and after RM-IV depositional times. In contrast, it was relatively warm during RM-II and RM-IV, when *Quercus* was predominant. Similarly, during the deposition of the earlier part of RM-II and after RM-IV, the climatic conditions were relatively wetter. In general, RM-I has relatively high amount of soft coercivity magnetic minerals compared to the other zones and it further reinforces the notion of the relatively cooler climate.

It has been mentioned earlier that the rockmagnetic parameters show broad changes taking place at every 4-m interval corresponding to zones from RM-I to RM-IV. In detail, however, each zone can be subdivided into 3 subzones (a, b and c); each subzone with a thickness of 1-2 m has rockmagnetic characteristics differing from the subzones below and above (Fig. 7). Pollen indices ('cold' and 'wet') would point out to fine metric-scale variations as shown by the rockmagnetic subzones although the exact relationship between such variations in pollen and RM subzones is difficult to establish. This problem in part arises due to the lower number of pollen levels studied and some uncertainties in correlation of the differing exposures used for taking pollen and rockmagnetic samples.

DISCUSSION AND CONCLUSIONS

Magnetic remanence data (section 4.2, above) revealed a characteristic remanence of consistently normal polarity throughout the section. The magnetic polarity sequence (mps) has no reversal attributable to the Laschamp event (Champion et al., 1988; dated at 41.1 kyrs BP as mentioned in Ogg, 2020) that was expected from some of the older radiocarbon dates presented earlier. Owing to the relatively short duration of the reversal event, possibility of depositional gaps in the sampled sediment column, and other factors that affect the preservation of a stable depositional remanence and its recovery, however, this mps may not be used to judge the validity of some of the older (i. e., predating the Laschamp event) radiocarbon dates.

The rockmagnetic zones distinguished in the Thimi section (Fig. 7) are based on small variations in the proportion of minerals differing in magnetic hardness and also the grain size. The rock magnetic boundary at 7 m may mark a significant change in the depositional system. As shown earlier, the *in situ* magnetic susceptibility is directly correlated to the macroscopic lithology and thus serves a powerful correlation tool. The distinct and consistently cyclic nature of the variations of several rockmagnetic parameters shown by the discretely sampled fine-grained black silt/clay layers, is indeed significant. Therefore, these parameters are useful for

quantifying subtle variations at a fine scale (i.e., even among the silt/clay layers that are a part of the sedimentary rhythms).

Although, there seems to be correspondence between the pollen zones and the rockmagnetic zones distinguished in this paper, the exact relationship between them can't be elaborated in absence of additional non-magnetic proxy parameters, e.g., sedimentological, geochemical and isotopic data. More importantly, it is desirable to have more precise age limits of the Thimi section so that these zones may be assigned temporal significance and additional techniques (e.g., time-series analysis) could be employed.

In conclusion, the minor variations in magnetic minerals (by type and grain size) within the layers constituting the younger stage clastic deposits of the Kathmandu valley are reflected in the rockmagnetic parameters. They exhibit cyclicity and zonation. Integration of these new data with continuous records of other non-magnetic parameters (sedimentological, geochemical, pollen, etc.) and geochronological data is believed to enable better reconstruction of the environmental/ climatic/hydrological conditions of the past in the Kathmandu basin.

ACKNOWLEDGEMENTS

This manuscript benefited from discussions with J. L. Mugnier, Grenoble and K. Arita, Sapporo. We appreciate expert advice of A.P. Gajurel during fieldwork in Kathmandu and Fabienne Vadeboin during laboratory measurements at CEREGE, France. PG was supported by Research Fellowships at the University of Joseph Fourier-Grenoble from both CNRS and Region Rhone Alpes as well as a JSPS Grant-in-aid for scientific research (kiban kenkyu C, No. 17540427) at Hokkaido University. Efficient editorial management of Ranjan Dahal together with comments from an anonymous reviewer led to the improvements in the manuscript.

REFERENCES

Champion, D.E., Lanphere, M.A. and Kuntz, M.A., 1988. Evidence for a new geomagnetic reversal from lava flows in Idaho: Discussion of short polarity reversals in the Brunhes and late Matuyama polarity chrons. Jour. Geophy. Res., v. 93, pp. 11667-11680. https://doi.org/10.1029/JB093iB10p11667.

Day, R., Fuller, M. and Schmidt, V.A., 1977. Hysteresis properties of titanomagnetites: grain-size and compositional dependence. Phy. Ear. Planet. Inter., v. 13, pp. 260-267. https://doi.org/10.1016/0031-9201(77)90108-X.

Dill, H. G., 2006. An overview of younger Kathmandu Lake, Nepal, during the Late Quaternary, with special reference to ferruginous structures in carbonaceous sediments. Inter. Geol. Rev., v 48(5), pp. 383-409. https://doi.org/10.2747/0020-6814.48.5.383.

Dill, H.G., Kharel, B.D., Singh, V.K., Piya, B., Busch, K. and Geyh, M., 2001. Sedimentology and paleogeographic evolution of the intermontane Kathmandu basin, Nepal, during the Pliocene and Quaternary. Implications for formation of deposits of economic interest. Jour. Asia. Ear. Sci., v. 19, pp. 777-804. https://doi.org/10.1016/S1367-9120(01)00011-6.

von Dobenec, T., 1996. A systematic analysis of natural magnetic mineral assemblages based on modeling hysteresis loops with coercivity-related hyperbolic basis functions. Geophy. Jour. Inter., v. 124, pp. 675-694. https://doi.org/10.1111/j.1365-246X.1996.tb05632.x.

Dunlop, D.J. and Ozdemir, O., 1997. Rock Magnetism: fundamentals and frontiers, Cambridge University Press. 573 p. https://doi.org/10.1017/CBO9780511612794.

Fujii, R., Kuwahara, S. and Sakai, H., 2001. Mineral composition changes recorded in the sediments from a 284-m-long drill-well in central part of the Kathmandu Basin. Jour. Nepal Geol. Soc., v. 25 (Sp. Issue), pp. 63-69. https://doi.org/10.3126/jngs.v25i0.32053

Fujii, R. and Sakai, H., 2001. Palynological study of the drilled sediments from the Kathmandu Basin and its palaeoclimatic and climatic significance. Jour. Nepal Geol. Soc., v. 25 (Sp. Issue), pp. 53-61. http://dx.doi.org/10.3126/jngs.v25i0.32052.

Gajurel, A.P., 1998, Geochemie isotopique et deformations synsedimentaires des depots du bassin de Kathmandou, Memoire de DEA de l'Universite de Grenoble, 306 p. (in French).

Gautam P. and Fujiwara, Y., 2000. Magnetic polarity stratigraphy of Siwalik Group sediments of Karnali River section in western Nepal. Geophy. Jour. Inter., v. 142, pp. 812-824. https://

doi.org/10.1046/j.1365-246x.2000.00185.x

Gautam, P., Hosoi, A., Sakai, T. and Arita, K., 2001. Magnetostratigraphic evidence for the occurrence of pre-Brunhes (>780 kyr) sediments in the northwestern part of the Kathmandu Valley, Nepal. Jour. Nepal Geol. Soc., 25 (Sp. Issue), pp. 99-109. http://dx.doi.org/10.3126/jngs.v25i0.32065.

Goddu, S.R., Appel, E., Gautam, P., Oches, E.A. and Wehland, F., 2007. The lacustrine section at Lukundol, Kathmandu basin, Nepal: Dating and magnetic fabric aspects. Jour. Asia. Ear. Sci., v. 30(1), pp. 73-81. https://doi.org/10.1016/j.jseaes.2006.07.009.

Hrouda, F., 1994. A technique for the measurement of thermal changes of magnetic susceptibility of weakly magnetic rocks by the CS-2 apparatus and KLY-2 Kappabridge, Geophy. Jour. Inter., v. 118, pp. 604-612. https://doi.org/10.1111/j.1365-246X.1994.tb03987.x.

Igarashi, Y., Yoshida, M. and Tabata, H., 1988. History of vegetation and climate in the Kathmandu valley. Proceedings of Indian National Science Academy, v. 54A(4), pp. 550-563. http://dx.doi.org/10.3126/bdg.v20i0.20722.

Kirschvink, J.L., 1980. The least-squares line and plane analysis of palaeomagnetic data. Geophy. Jour. of the Roy. Astrono. Soc., v. 62, pp. 699-718. https://doi.org/10.1111/J.1365-246X.1980.TB02601.X.

Kuwahara, Y., Fujii, R., Sakai, H. and Masudome, Y., 2001. Measurements of crystallinity and relative amount of clay minerals in the Kathmandu Basin sediments by decomposition of XRD patterns (profile fitting). Jour. Nepal Geol. Soc., v. 25 (Sp. Issue), pp. 71-80.

Mugnier, J.L., Huyghe, P., Gajurel, A.P., Upreti, B.N. and Jouanne, F., 2011. Seismites in the Kathmandu basin and seismic hazard in central Himalaya. Tectonophy., v. 509(1-2), pp. 33-49. http://dx.doi.org/10.1016/j.tecto.2011.05.012

Ogg, J., 2020. Geomagnetic Polarity Time Scale. In: Gradstein, F.M. et al. (eds.), A Geologic Time Scale 2020. Elsevier. DOI: 10.1016/B978-0-12-824360-2.00005-X.

Paudayal, K.N., 2005. Late Pleistocene pollen assemblages from the Thimi Formation, Kathmandu Valley, Nepal. Isla. Arc., v. 14(4), pp. 328-337. http://dx.doi.org/10.1111/j.1440-1738.2005.00490.x

Paudayal, K.N. and Ferguson D.K., 2004. Pleistocene palynology of Nepal. Quarter. Inter., v. 117(1), pp. 69-79. https://doi.org/10.1016/S1040-6182(03)00117-4.

Paudel, M.R., 2022. Marginal fan thick lacustrine sedimentation: Implication for tectonics and/or climatic causes in Kathmandu basin. Jour. Nepal Geol. Soc., v. 63(1), pp. 61–70. https://doi.org/10.3126/jngs.v63i01.50842

Polunin, O. and Stainton, A., 1984. Flowers of the Himalaya, Oxford, 580 p.

Sakai, H., 2001. The Kathmandu Basin: an archive of Himalayan uplift and past monsoon climate. Jour. Nepal Geol. Soc., v. 25 (Sp. Issue), pp. 1-8. https://doi.org/10.3126/jngs.v25i0.32032.

Sakai, H., Fujii, R., Sugimoto, M., Setoguchi, R. and Paudel, M.R., 2016. Two times lowering of lake water at around 48 and 38 ka, caused by possible earthquakes, recorded in the Paleo-Kathmandu lake, central Nepal Himalaya. Earth Plan. Spa., v. 68, Ar. 31, pp. 1-10. http://dx.doi.org/10.1186/s40623-016-0413-5.

Sakai, H., Sakai, H., Yahagi, W., Fujii, R., Hayashi, T. and Upreti, B. N., 2006. Pleistocene rapid uplift of the Himalayan frontal ranges recorded in the Kathmandu and Siwalik basins. Palaeogeo. Palaeocli. Palaeoeco., v. 241(1), pp. 16-27. http://dx.doi.org/10.1016/j.palaeo.2006.06.017.

Sakai, T. Gajurel, A.P., Tabata, H. and Upreti, B.N., 2001. Small-amplitude lake level fluctuations recorded in aggrading deltaic deposits of the Upper Pleistocene Thimi and Gokarna Formations, Kathmandu Valley. Jour. Nepal Geol. Soc., v. 25 (Sp. Issue), pp. 43-51. http://dx.doi.org/10.3126/jngs.v25i0.32049.

Verosub, K.L. and Roberts, A.P., 1995. Environmental magnetism: Past, present, and future. Jour. Geophy. Res. 100(B2), pp. 2175-2192. https://doi.org/10.1029/94JB02713.

Yoshida, M. and Gautam, P., 1988. Magnetostratigraphy of Plio-Pleistocene lacustrine deposits in the Kathmandu valley, central Nepal. Proceedings of Indian National Science Academy, v. 54A(3), pp. 410-417.

Yoshida, M. and Igarashi, Y., 1984. Neogene to Quaternary lacustrine sediments in the Kathmandu valley, Nepal. Jour. Nepal Geol. Soc., v. 4(Sp. Issue), pp. 73-100.